Computational Fluid Dynamics Analysis of Flow in a Straight Flume for Sediment Erodibility Testing

Thomas M. Ravens[1] and Richard A. Jepsen[2]

Abstract: Computational fluid dynamics calculations of flow in a straight flume for sediment erodibility testing were conducted. The calculations allowed improved postprocessing of the erosion data collected and better understanding of scour pit formation that is sometimes found in the flume's test section. The flume is a 3-m-long, rectangular (13-cm-wide by 10-cm-high) water conduit, which is placed on the sediment water interface during the sediment transport tests. The flume consists of a 1.6-m inlet section, followed by a 1.1-m test section, where the flowing water contacts the sediment. After erosion has occurred in the test section, the flow entering from the inlet section is an expanding flow. It generates a circulation cell and nonuniform bottom stress and pressure. Flow calculations were conducted for four different erosion depths (0, 1, 2, and 4 cm) and for two different flow velocities (1 and 0.5 m/s). After erosion had occurred, the effective stress in the test section was within 15% of the bottom stress calculated with the Schlichting equation, as long as the increased cross-sectional area was accounted for.

DOI: 10.1061/(ASCE)0733-950X(2006)132:6(457)

CE Database subject headings: Flumes; Cohesive sediment; Computational fluid dynamics technique; Shear strength; Shear stress; Erosion.

Introduction

Knowledge of the erodibility of cohesive sediments (the rate of erosion as a function of hydraulic conditions) is necessary for conducting fate and transport studies of particle-bound contaminants and for developing sediment budgets. Unfortunately, cohesive sediment erodibility is not easily predictable based on environmental data (McCave 1984; Aberle et al. 2004). As a consequence, a number of devices have been developed in order to measure sediment erodibility directly. These devices include: annular flumes (Amos et al. 1992; Maa et al. 1993), straight flumes (Young 1975; Gust and Morris 1989; McNeil et al. 1996; Ravens and Gschwend 1999; Aberle et al. 2004), the Shaker test (Tsai and Lick 1986), and others (Lee and Mehta 1994). While these devices have provided useful information on sediment erodibility, they often have limitations. For example, laboratory flumes are limited as it is difficult to bring sediment cores into the lab without disturbing them. Other devices, (e.g., the Shaker test) have been criticized, as the turbulence used to generate erosion is quite different from that observed in nature.

Here, we address the limitations of a straight flume that is deployed in situ in order not to disturb the sediments (Fig. 1). The flume is 3-m long with a rectangular cross-section (13-cm wide by 10-cm high). It is modeled after the flume described by Ravens and Gschwend (1999). The flume is placed on the sediments of interest and water is pulled through the flume by an onboard pump. The flume features a 1.6-m inlet section, with a boundary layer trip to stimulate development of the boundary layer and a floor to prevent erosion of sediment before it is fully developed. Following the inlet section is the 1.1-m sediment test section where the floor is removed and the flowing water is allowed to contact and erode the sediment. The flume is operated at different flow rates corresponding to different bottom stresses, and the erosion rate is observed as a function of bottom stress. The erosion rate is determined based on the particle concentration and the flow rate. When there is negligible erosion in the test section, the bottom stress can be calculated based on the average flow velocity, U, according to

$$\tau = \rho \frac{f}{8} U^2 \tag{1}$$

where ρ=fluid density (kg/m^3) and f=friction factor. The friction factor can be obtained through the Schlichting equation (Schlichting 1979; McNeil et al. 1996), assuming smooth walls

$$\frac{1}{\sqrt{f}} = 2.0 \log(\mathrm{R}\sqrt{f}) - 0.8 \tag{2}$$

where R=Reynolds number ($=UD/\nu$); D=equivalent diameter of the rectangular conduit ($D=4A/P$); A=cross-sectional area; P=wetted perimeter; and ν=kinematic viscosity (m^2/s).

After the sediment has eroded from the sediment test section, the flow of water entering the test section is an expanding flow. As a consequence, the Schlichting equation, which assumes fully developed flow, becomes invalid, and the bottom stress in the test section becomes uncertain. In this paper, a computational fluid dynamics (CFD) model is used to calculate the effective bottom stress in the test section after erosion has occurred. The model is

[1]Assistant Professor, Dept. of Maritime Systems Engineering, Texas A & M Univ., P.O. Box 1675, Galveston TX 77553 (corresponding author). E-mail: ravenst@tamug.edu

[2]Technical Staff, Sandia National Laboratories, P.O. Box 5800, MS 1135, Albuquerque, NM 87185. E-mail: rajepse@sandia.gov

Note. Discussion open until April 1, 2007. Separate discussions must be submitted for individual papers. To extend the closing date by one month, a written request must be filed with the ASCE Managing Editor. The manuscript for this paper was submitted for review and possible publication on January 25, 2005; approved on January 17, 2006. This paper is part of the ***Journal of Waterway, Port, Coastal, and Ocean Engineering***, Vol. 132, No. 6, November 1, 2006. ©ASCE, ISSN 0733-950X/2006/6-457–461/$25.00.

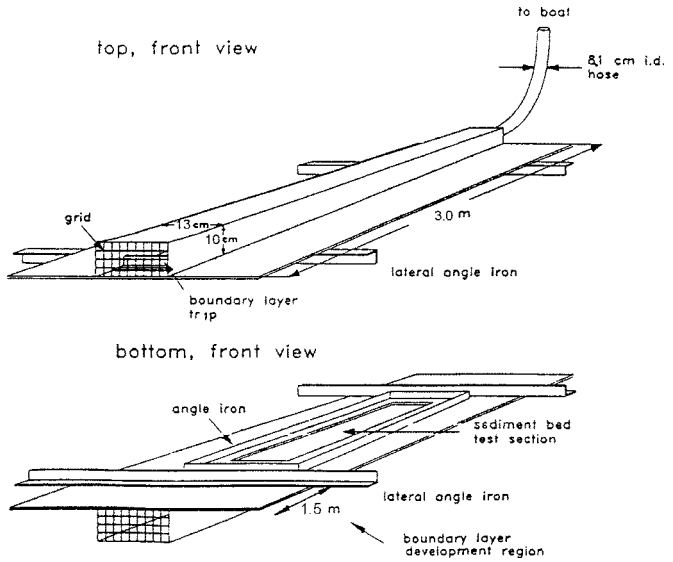

Fig. 1. Schematic of in situ straight flume (adapted from Ravens and Gshwend 1999)

also used to gain insight into the scour pits that sometimes develop near the entrance and exit of the test section (Fig. 2). With this flume, scour pits are mainly seen when studying soft sediments and for erosion depths greater than 4 cm. Similar scour pits appear to be present in other straight flumes including the laboratory SEDFLUME (McNeil et al. 1996) and another straight, in situ flume (Aberle et al. 2004).

Methods and Results

CFD Analysis of Flow within Flume

A two-dimensional CFD model was developed and used to study the hydrodynamics in the flume. The model was executed using Adaptive Research Storm/CFD2000 version 4.1 software on a 2.5 GHz processor using Windows 2000. The model calculates the time-averaged velocity and pressure in the flume based on the conservation of mass and linear momentum equations and based on initial and boundary conditions. The turbulent viscosity, μ_T, (used in the conservation of momentum equation) was obtained using the standard k-ε turbulence model (Launder and Spaulding 1974)

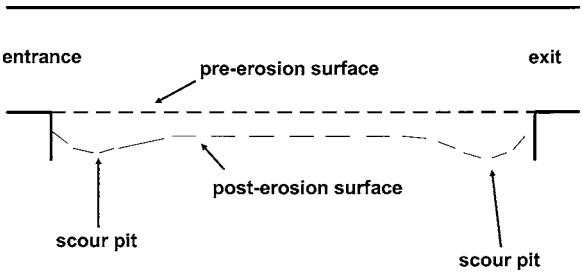

Fig. 2. Schematic of flume test section (side view) showing pre- and post-erosion sediment surfaces and location of scour pits

Table 1. k-ε Turbulence Model Constants

C_μ	C_1	C_2	Pr_k	Pr_ε
0.09	1.44	1.92	1.0	1.3

$$\mu_T = \frac{C_\mu \rho k^2}{\varepsilon} \tag{3}$$

where C_μ=dimensionless constant (Table 1); ρ=local density; k=specific turbulent kinetic energy; and ε=turbulent energy dissipation rate. The specific turbulent kinetic energy and the turbulent energy dissipation rate were calculated using the following transport equations:

$$\frac{\partial \rho k}{\partial t} + \frac{\partial (\rho u_i k)}{\partial x_i} = \frac{\partial}{\partial x_i}\left[\left(\mu + \frac{\mu_T}{\mathrm{Pr}_k}\right)\frac{\partial k}{\partial x_i}\right] + \mu_T G - \rho\varepsilon + S_{k,p} \tag{4}$$

$$\frac{\partial \rho \varepsilon}{\partial t} + \frac{\partial (\rho u_i \varepsilon)}{\partial x_i} = \frac{\partial}{\partial x_i}\left[\left(\mu + \frac{\mu_T}{\mathrm{Pr}_\varepsilon}\right)\frac{\partial \varepsilon}{\partial x_i}\right] + \frac{\varepsilon}{k}(C_1 \mu_T G - C_2 \rho\varepsilon) + S_{\varepsilon,p} \tag{5}$$

where C_1 and C_2=dimensionless constants and Pr_k and Pr_ε=turbulent Prandtl numbers for kinetic energy and dissipation; $S_{k,p}$ and $S_{\varepsilon,p}$=source terms for the kinetic energy and turbulent dissipation; and G=turbulent production rate described by

$$G = \left(\frac{\partial u_i}{\partial x_j} + \frac{\partial u_j}{\partial x_i}\right)\frac{\partial u_i}{\partial x_j} - \frac{1}{\rho^2}\frac{\partial \rho}{\partial x_j}\frac{\partial p}{\partial x_j} - \frac{2}{3}\left(\frac{\partial k}{\mu_T} + \frac{\partial u_i}{\partial x_j}\right)\frac{\partial uj}{\partial x_j} \tag{6}$$

The values for the dimensionless constants are given in Table 1 based on Launder et al. (1972). The model was used to calculate the flow velocity and pressure throughout the flume interior including the boundary layer. The shear stress was calculated during post processing from the velocity profile in the viscous sublayer at the sediment–water interface [Eq. (8)]

$$\tau = \mu \frac{\partial u}{\partial y} \tag{7}$$

where u=local velocity (m/s); and μ=dynamic viscosity (kg/m s).

The geometry and grid used for the model study is shown in Fig. 3. The geometry was divided into three horizontal sections representing the flume inlet channel, test section and the outlet section. The geometry was also set up such that up to 4 cm of erosion could be studied in 1-cm increments. Therefore, five vertical regions were defined for the channel height and the four erosion scenarios. The grids within each region were defined individually to provide a fine mesh near the wall in the test section for accurate boundary layer representation and a coarse mesh in the inlet and outlet sections of the flume where the interactions with the wall are not as important. This optimized the run time for the model calculation while providing a high-resolution mesh in the area of interest.

In all cases, the sediment water interface was modeled as completely flat or horizontal. Therefore, differences in erosion depth (e.g., scour pits) that are sometimes seen in the test section, were not accounted for. Instead of modeling the actual inlet section with its boundary layer trips, for simplicity, a 3-m-long inlet section (long enough to allow full development of the flow) was used.

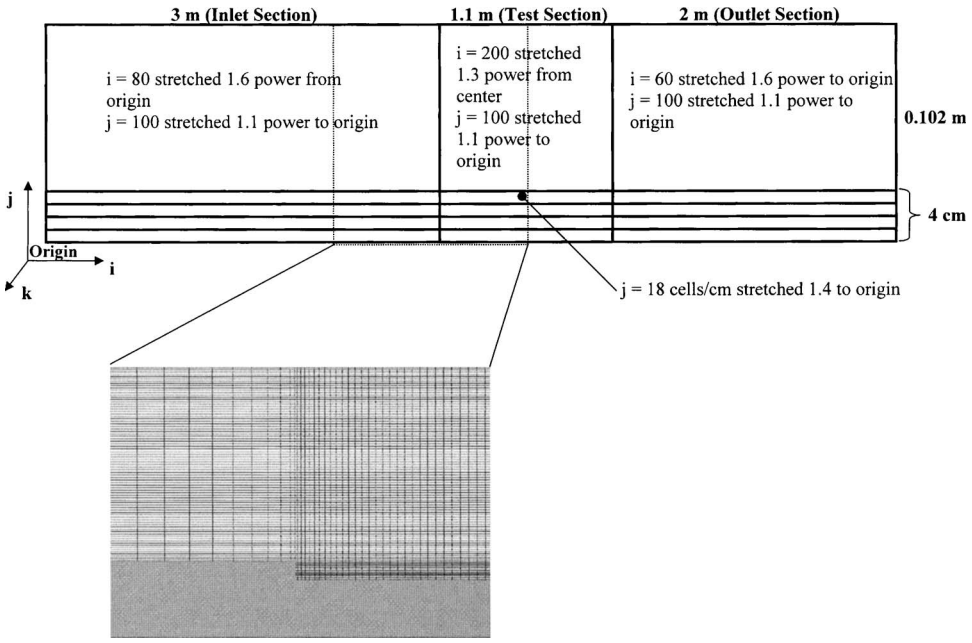

Fig. 3. Geometry and grid used in modeling study (figure is not to scale)

Results of CFD Analysis

CFD analysis was performed for 0, 1, 2, and 4 cm of erosion at 1 m/s inlet velocity and for 0 and 2 cm of erosion at 0.5 m/s inlet velocity. Bottom stress [from Eq. (8)] and pressure were found to be spatially variable in the test section (Fig. 4). In all erosion cases there was a peak in bottom stress in the second (downstream) half of the test section. At the same location there was a minimum in pressure. This is one location where scour pits have been reported (Ravens and Gschwend 1999; Aberle et al. 2004). In addition, the bottom stress and pressure, respectively, exhibit a minimum (which was negative) and a maximum, just downstream of the inlet of the test section. This is another location of scour pit formation (Ravens and Gschwend 1999). The negative bottom stress just downstream of the inlet results from negative near-bottom velocity due to a clockwise circulation cell near the sediment–water interface (Fig. 5). The circulation cell was observed in all erosion cases studied. The circulation created a diverging flow at the sediment water interface, near the location of the pressure maximum. The average velocity and bottom shear stress magnitude is reduced in this region (Fig. 4). The extent of the circulation cell into the test section increased with inlet velocity and erosion depth (Table 2). The extent of the circulation cell was consistent with experimental work on flow over a backward facing step reviewed and conducted by Adams and Johnston (1988). According to these sources, for Reynolds numbers ranging from 40,000 to 100,000, and with upstream boundary layer thicknesses of the same order as the step height (H), the reattachment distances should be between 6 and 7 H.

Based on the bottom stress distribution data (Fig. 4), the aver-

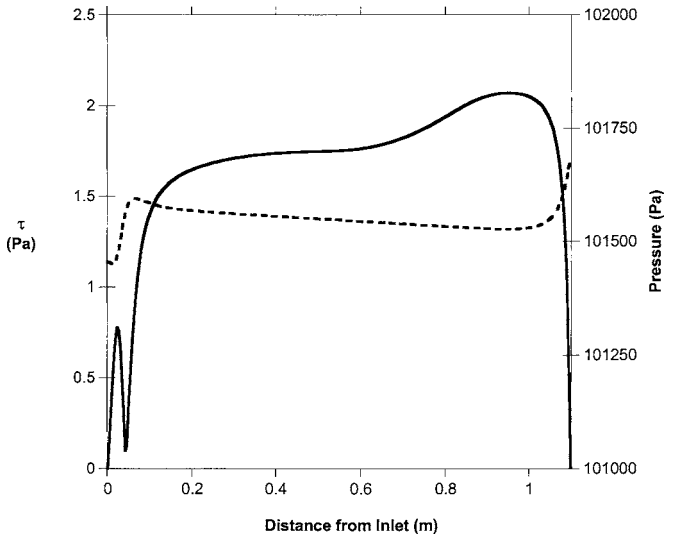

Fig. 4. Model-calculated bottom shear stress (——) and pressure (----) for 1 cm erosion at 1 m/s average flow velocity

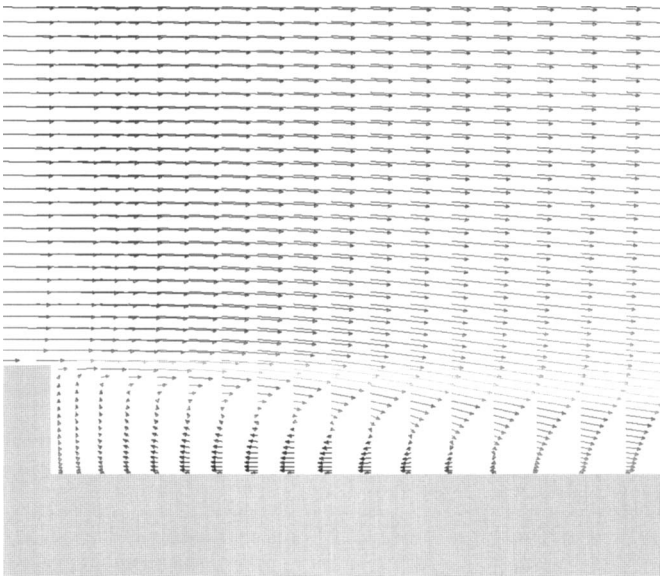

Fig. 5. Blowup of test section inlet. Circulation cell shown by velocity vectors for 2 cm erosion at 1 m/s average flow velocity.

Table 2. Horizontal Extent of Circulation Cell by Inlet of Test Section for Different Erosion Scenarios Studied

Average inlet velocity (m/s)	Depth of erosion (cm)	Horizontal extent of circulation cell (cm)
1.0	1	5
1.0	2	9
1.0	4	19
0.5	2	8

age stress, the peak stress, and the root mean square (RMS) of the bottom stress in the test section were calculated for all of the scenarios tested (Table 3). The rms stress is the effective stress in the test section assuming that erosion rate is related to the square of the bottom stress (McNeil et al. 1996, Ravens, private communication). In all cases, the average, the peak, and the rms shear stress decreased with increasing erosion in the test section (Table 3).

Discussion

Interpretation of CFD Results

The CFD-based stress calculations were compared with the stress as calculated with the Schlichting equation for the six different scenarios (Table 3). Note, in the four instances in which sediment had eroded from the test section, the cross-sectional area in the test section was increased. Increasing the cross-sectional area reduces the average velocity and increases the effective diameter of the conduit. Both of these changes affect the drag coefficient and the bottom stress generated by the Schlichting equation. The data indicates that the Schlichting equation generates a stress that approximates the CFD-based stress (average and RMS). However, as one might expect, the Schlichting equation under calculates the peak stress (as calculated by CFD) by as much as 36%. Focusing on the RMS stress calculation, there was relatively little disagreement with the Schlichting equation (maximum error $<15\%$). Therefore, the results indicate that the effective bottom stress in the test section, following modest amounts of erosion, can be reasonably estimated with the Schlichting equation despite the fact that circulation cells exist and the flow is not fully developed. Note, if the Schlichting equation was used to calculate bottom stress (as opposed to using the CFD-calculated stress), an error would effectively be introduced into the measured erosion rate relationship. If the erosion rate was a linear function of bottom stress, the error in the measured rate would be less than 15%. If the erosion rate was a quadratic function of stress, the error in the measured rate would be less than 28%. These error rates are actually fairly small. A recent comparison of erosion rates from two different flumes found a sixfold difference in measured erosion rate (Ravens, private communication). Further, the measured erosion rates are spatially heterogeneous, varying by as much as 50% only a few meters away.

The analysis also provided insight into the two locations—near the entrance and exit of the test section—where scour pits have sometimes been observed (Fig. 2). The location of the exit scour pit coincided with a peak in bottom stress and with a minimum in bottom pressure. Since the erosion rate typically goes as the bottom stress to some power (>1), the near exit scour pit makes sense. The presence of a pressure minimum could potentially enhance particle erosion by generating an upward porewater velocity and an upward force on the sediment aggregates.

The location of the entrance scour pit coincided with a circulation cell that created a diverging flow and maximum in bottom pressure. Interestingly, the calculation of the time-averaged bottom shear stress at this location (based on the time-averaged velocity) indicates relatively little shear stress. Hence, scour can occur in locations where the time-averaged bottom shear stress is not very great, though velocity and pressure fluctuations and instantaneous stresses may be great. We note that our model did not allow calculation of the instantaneous conditions.

Dey and Westrich (2003) experimentally studied scour holes in cohesive sediments downstream of an apron subject to a submerged horizontal jet. This is a flow/sediment transport situation very similar to the one at hand. Using velocity measurements, they similarly documented a circulation cell at the location of the scour hole. Calculations of bottom stress (based on the velocity measurements) indicated a relatively low bottom stress in the scour hole. Hence, their results also indicate that scour can occur even when the mean shear stress is relatively low.

Blaisdell et al. (1981) and Stein et al. (1993) studied scour due to an impinging jet in plunge pools. This is a flow/sediment transport situation resembling the one at hand. Working with cohesionless sediments, they found that sediment particles can be detached and entrained by the fluctuating velocity and pressure of the jet even when the mean shear stress was less than the critical shear stress. In cohesive sediments, fluctuating pressures can generate enhanced pore pressures which eventually lead to liquefaction and scour (Sumer and Fredsoe 2002). Hence, in a nonuniform

Table 3. Comparison of CFD-Based Calculations of Test-Section Bottom Shear Stress (Average, Peak, and RMS) with Calculations Based on Schlichting Equation

Average inlet velocity (m/s)	Erosion depth (cm)	Average test section velocity (m/s)	Average shear stress for test section from CFD (Pa)	Peak shear stress in test section from CFD (Pa)	rms shear stress in test section from CFD (Pa)	Shear stress (Schlichting) (Pa)
1	0	1.00	2.15	2.15	2.15	1.95
1	1	0.91	1.34	2.05	1.41	1.61
1	2	0.84	1.15	1.85	1.25	1.36
1	4	0.72	1.05	1.56	1.18	1.00
0.5	0	0.50	0.71	0.71	0.71	0.56
0.5	2	0.42	0.42	0.54	0.45	0.39

flow situation such as that seen at the entrance of the sediment test section, other flow properties besides the mean bottom stress are probably driving the sediment erosion.

One question raised by this analysis is the relevance of the mean and/or the RMS bottom stress that we calculated based on the CFD results. One might argue that since the scour hole formation that occurs near the inlet of the test section is happening in a "low-stress" environment, we are somehow undercalculating the "effective" stress in this region. There is a ring of truth here. In practical operation of the flume, however, we aim to avoid conducting tests where significant scour holes are forming mainly because we have no confidence that we understand the effective stress if scour pits are forming. If scour pits have not formed, and if the amount of erosion is quite limited (e.g., 1 cm), then we have confidence that the bottom stress is fairly uniform since the rate of erosion has been fairly uniform. In this circumstance, we would like to know the effective stress and we can turn to these CFD-based results for an answer.

Conclusion

The results presented here have important implications for the operation of the particular type of straight flume under consideration. They indicate that, if the amount of erosion in the test section is accounted for by increasing the cross-sectional area, the Schlichting equation will provide a reasonably accurate equation for the effective shear stress in the test section (assuming the sediment surface is fairly flat as assumed in the model). In addition, the results shed light on some of the causes of variable erosion sometimes seen in the test section, especially at erosion depths greater than 4 cm. The existence of a circulation cell accompanied by diverging flow and a peak in bottom pressure by the inlet of the test section is undoubtedly related to the observation of scour pits there. It is noteworthy that this scour hole develops in a low average shear stress environment. Hence, other mechanisms of sediment scour are at play. The peak in bottom stress near the test section exit is likely responsible for scour pits sometimes observed at that location.

Acknowledgments

Sandia National Laboratories is a multiprogram laboratory operated by Sandia Corporation, a Lockheed Martin Company, for the United States Department of Energy under Contract No. DE AC04-94AL85000.

Notation

The following symbols are used in this paper:

A = cross-sectional area (m^2);
C_1, C_2, C_μ = dimensionless constants;
D = equivalent diameter of conduit (m);
f = friction factor (dimensionless);
G = turbulent production rate (s^{-2});
H = height of backward facing step (m);
k = specific turbulent kinetic energy (W/kg);
P = wetted perimeter (m);
Pr_k = turbulent Prandtl numbers for kinetic energy;
Pr_ε = turbulent Prandtl numbers for dissipation;
p = pressure (Pa);
$S_{k,p}$ = source term for kinetic energy ($W\,m^{-3}\,s^{-1}$);
$S_{\varepsilon,p}$ = source term for turbulent dissipation ($W\,m^{-3}\,s^{-1}$);
U = cross-sectional area-averaged velocity ($m\,s^{-1}$);
u = local velocity (m/s);
u_i = indicial velocity (m/s);
x_i = indicial position (m);
ε = energy dissipation rate (W/kg);
μ = dynamic viscosity ($kg\,m^{-1}\,s^{-1}$);
μ_T = turbulent viscosity ($kg\,m^{-1}\,s^{-1}$);
ν = kinematic viscosity (m^2/s);
ρ = water density ($kg\,m^{-3}$); and
τ = bottom shear stress (Pa).

References

Aberle, J., Nikora, V., and Walters, R. (2004). "Effects of bed material properties on cohesive sediment erosion." *Mar. Geol.*, 207(1–4), 83–93.

Adams, E. W., and Johnston, J. P. (1988). "Effects of the separating shear layer on the reattachment flow structure. Part 2: Reattachment length and wall shear stress." *Exp. Fluids*, 6(7), 493–499.

Amos, C. L., Grant, J., Daborn, G. R., and Black, K. (1992). "SEA CAROUSEL—A Benthic, annular flume." *Estuarine Coastal Shelf Sci.*, 34(6), 557–577.

Blaisdell, F. W., Hebaus, G. G., and Anderson, C. L. (1981). "Ultimate dimensions of local scour." *J. Hydr. Div.*, 107(3), 327–337.

Dey, S., and Westrich, B. (2003). "Hydraulics of submerged jet subject to change in cohesive bed geometry." *J. Hydraul. Eng.*, 129(1), 44–53.

Gust, G., and Morris, M. J. (1989). "Erosion thresholds and entrainment rates of undisturbed in-situ sediments." *J. Coastal Res.*, 5, 87–99.

Launder, B. E., Morse, A., Rodi, W., and Spalding, D. B. (1972). "The prediction of turbulent free shear flows—A comparison of the performance of six turbulence models." *Proc., NASA Conf. on Free Shear Flows*, NASA Langley Research Center, Hampton, Va., 361–422.

Launder, B. E., and Spalding, D. B. (1974). "The numerical computation of turbulent flows." *Comput. Methods Appl. Mech. Eng.*, 3, 269–289.

Lee, S.-C., and Mehta, A. J. (1994). "Cohesive sediment erosion." *Dredging Research Program, DRP 94-6*, U.S. Army Corps of Engineers, Vicksburg, Miss.

Maa, J. P.-Y., Wright, L. D., Lee, C.-H., and Shannon, T. W. (1993). "VIMS sea carousel: A field instrument for studying sediment transport." *Mar. Geol.*, 115(3–4), 271–287.

McCave, I. N. (1984). "Erosion, transport, and deposition of fine-grained marine sediments." *Fine-grained sediments: Deep-water processes and facies*, D. A. V. Stow and D. J. W. Piper, eds., Blackwell Scientific, Oxford, U.K., 35–69.

McNeil, J., Taylor, C., and Lick, W. (1996). "Measurements of erosion of undisturbed bottom sediments with depth." *J. Hydraul. Eng.*, 122(6), 316–324.

Ravens, T. M., and Gschwend, P. M. (1999). "Flume measurements of sediment erodibility in Boston Harbor." *J. Hydraul. Eng.*, 125(10), 998–1005.

Schlichting, H. (1979). *Boundary layer theory*, McGraw–Hill, New York.

Stein, O. R., Julien, P. Y., and Alonso, C. V. (1993). "Mechanics of jet scour downstream of a headcut." *J. Hydraul. Res.*, 31(6), 723–738.

Sumer, B. M., and Fredsoe, J. (2002). *The mechanics of scour in the marine environment*, World Scientific, River Edge, N.J.

Tsai, C.-H., and Lick, W. (1986). "A portable device for measuring sediment resuspension." *J. Great Lakes Res.*, 12(4), 314–321.

Young, R. A. (1975). "Flow and sediment properties influencing erosion of fine-grained marine sediments: Sea floor and laboratory experiments." Ph.D. dissertation, Woods Hole Oceanographic Institution, Woods Hole, Mass.